Plasmonic Assemblies of Gold Nanorods on Nanoscale Patterns of Poly(ethylene glycol): Application in Surface-Enhanced Raman Spectroscopy

Sema Karabel Ocal,[1] Javier Patarroyo,[2] N. Burak Kiremitler,[1] Sami Pekdemir,[1] Victor F. Puntes,[2,3,] and M. Serdar Onses[1,*]*

[1] Department of Materials Science and Engineering, Nanotechnology Research Center (ERNAM), Erciyes University, Kayseri, 38039, Turkey

[2] Catalan Institute of Nanoscience and Nanotechnology (ICN2), CSIC and BIST, Campus UAB, Bellaterra, 08193 Barcelona, Spain

[3] Institució Catalana de Recerca i Estudis Avançats (ICREA), 08010 Barcelona, Spain

* Address correspondence to: onses@erciyes.edu.tr, victor.puntes@icn2.cat

ABSTRACT

Approaches are needed for the tailored assembly of plasmonic building blocks on the surface of substrates to synergistically enhance their properties. Here we demonstrate selective immobilization and assembly of gold nanorods (NRs) on substrates modified and patterned with end-grafted poly(ethylene glycol) (PEG) layers. The ligand exchange from the initial cetyltrimethylammonium bromide to sodium citrate was necessary for the immobilization of gold NRs onto PEG grafted substrates. Linear nanopatterns of PEG were fabricated using electrospun nanofibers as masks in oxygen plasma etching. The selective immobilization of citrate-stabilized gold NRs with a length of ~50 nm and a width of 20 nm on the nanopatterned PEG layers led to linear and registered arrays of rods. The number of gold NRs per line depended on the width of the patterns and approached 1 when the width of the patterns was comparable to the length of the rods. The confinement of the binding regions led to a ~3 fold increase in the number of gold NRs immobilized per unit area. The selective and dense immobilization of gold NRs on the nanoscale patterns of PEG resulted in spatially defined and strong surface-enhanced Raman scattering activity enabling detection of molecules at concentrations as low as 1 nM.

KEYWORDS: gold nanorods; SERS; nanofabrication; plasmonics; end-grafted polymers

1. Introduction

Plasmonic nanostructures exhibit unique optical properties that show great promise for a broad range of applications in molecular sensing [1], anti-counterfeiting [2], photovoltaics [3] and catalysis [4]. The optical properties of noble metal nanostructures are dominated by localized surface plasmons which can be tuned by the material composition, size, geometry and surface state of the particles [5]. Anisotropic nanoparticles (NPs), such as gold nanorods (NRs), provide additional means to control surface plasmon resonances: The asymmetric axes of the rods result in two distinct plasmon modes, namely longitudinal and transverse, whose location can be tuned through the engineering of the diameter and aspect ratio of NRs [6]. More interestingly, assemblies of metallic NPs lead to collective properties, which depend on the topographical distribution and spacing between the particles [7, 8]. Thus, the strong localization and focusing of light between the metallic NPs separated by a few nanometers results in a hot spot of high concentration of the electromagnetic field. In the case of anisotropic NPs, intense electric fields also arise near the sharp edges of the particles as a function of the orientation and spacing between the particles [9, 10]. Such hot spots enable electromagnetic enhancement of Raman scattering and allow for sensing of low concentrations of molecules via surface-enhanced Raman spectroscopy (SERS) [11, 12]. As a highly sensitive, nondestructive and label-free technique, SERS has found applications in a broad range of fields including food safety, biomedical technologies and diagnostics [13-15]. These and other applications motivate the development of techniques for inexpensive and scalable fabrication of plasmonic nanostructures with engineered optical properties.

Top-down engineering approaches, such as electron beam lithography together with metal evaporation, allow for spatially defined metallic nanostructures with a certain level of control over the size and geometry of the particles [16, 17]. However, it is extremely difficult to fabricate nanostructures with single crystallinity and molecularly defined roughness in 3D geometries and complex structures using these top-down approaches. Therefore, a bottom-up route to such nanostructures involves wet-chemical methods to synthesize colloidal NPs and their posterior organization in the desired structures [18, 19]. In addition to their superior properties, such as single crystallinity and molecular roughness, wet-chemical methods can be easily scaled up to produce massive amounts of colloidal nanomaterials with precise control over their size, shape, and composition [20, 21]. The utilization of the unique plasmonic properties of colloidal NPs in practical device applications requires uniform immobilization and assembly of the metallic nanostructures on a solid substrate in a dry state with control over the collective properties of the particle assemblies.

Substrates modified with end-grafted poly(ethylene glycol) (PEG), in particular, have recently gained significant interest for immobilization and assembly of gold NPs. Despite the wide-spread usage of PEG in surface modification for prevention of non-specific adsorption of biomolecules in biotechnology applications, [22] the capability of PEG brushes for uptake of gold NPs is relatively new. Vaia and coworkers [23] showed that citrate-stabilized Au NPs could be effectively immobilized on surfaces functionalized with end-grafted chains of PEG. Interestingly, binding affinity strongly depended on the size of the particle and the molecular weight of PEG grafts. This aspect, together with nanopatterning, enabled fabrication of different plasmonic heterostructures [24, 25]. Several other reports [26-33] employed PEG containing thin films to immobilize and assemble citrate-stabilized gold NPs. Despite the growing interest in PEG for

surface assembly of plasmonic structures, previous efforts have been limited to nanoscale building blocks consisting of spherical particles. However, the ability to assemble nanoscale building blocks of varying geometry, structure and composition is critically important for engineering the collective properties of plasmonic nanostructures.

This study presents the immobilization and assembly of gold NRs on homogenous and patterned layers of end-grafted PEG. We first investigated the binding of colloidal gold NRs stabilized with cetyltrimethylammonium bromide (CTAB) and citrate. For this purpose, CTAB-stabilized gold NRs were synthesized via a seed-mediated growth approach. Citrate-stabilized gold NRs were prepared via a ligand exchange process using the CTAB-stabilized rods. The stabilization of gold NRs with citrate allowed, for the first time, immobilization of anisotropic NPs on end-grafted PEG layers. Based on this selective binding, we investigated directed self-assembly of gold NRs on nanopatterned substrates. Linear patterns of PEG with nanoscale widths were prepared by the use of aligned nanofibers as etch masks. The assembly of citrate-stabilized gold NRs over the patterned regions facilitated close-placement of the particles with significantly higher densities accompanied with stronger SERS effects compared to homogenous PEG layers.

2. Experimental

2.1. Synthesis of CTAB and Citrate-Stabilized Gold Nanorods

Gold NRs stabilized with CTAB were synthesized by a method adapted from a previously published seed-mediated growth protocol [34]. An aqueous solution (5 mL, 0.20 M) of CTAB (Sigma-Aldrich) was mixed with $HAuCl_4$ (5 mL, 0.5 mM, Sigma-Aldrich) to prepare the seed solution. An ice-cold solution of $NaBH_4$ (0.60 mL, 0.01 M, Sigma-Aldrich) was added to the seed solution, resulting in a brownish yellow color. After 2 min of vigorous stirring, the seed solution

was kept at 25 °C and used within 2 h. For the growth solution, CTAB (5 mL, 0.20 M) was mixed with $AgNO_3$ (0.15 mL, 4 mM, Sigma-Aldrich) and $HAuCl_4$ (5 mL, 1mM), and a solution of ascorbic acid (60 μL, 0.1 M, Sigma-Aldrich) was then added. Ascorbic acid is a mild reducing agent and changed the growth solution from dark yellow to colorless. The final step was the addition of 20 μL of the seed solution to the growth solution. The ligand exchange from CTAB-stabilized to citrate-stabilized gold NRs via intermediate treatment with polystyrenesulfonate (PSS, Sigma-Aldrich) was performed following the procedure described by Wei and coworkers [35].

2.2. Characterization of gold NRs

Absorption spectra of the as synthesized and surfactant exchanged gold NRs were acquired with a Shimadzu UV-2401 PC spectrophotometer (Japan). The morphology and size of the gold NRs were visualized using a FEI Magellan XHR SEM (USA), in transmission mode operated at 20 kV. A droplet of the sample was drop cast onto a piece of ultrathin carbon-coated 200-mesh copper grid (Ted-Pella, Inc.) and left to dry in air. Zeta potential measurements were performed with Zetasizer Nano from Malvern (UK).

2.3. Preparation of Substrates and Immobilization of NPs

Silicon substrates were functionalized with PEG (M_n = 35.0 kg/mol, PDI = 1.15, Polymer Source Inc.) by a grafting to approach as described in our previous studies [36]. Briefly, a ~120 nm film of PEG was deposited on the freshly cleaned (UV-Ozone for 20 min) silicon substrate via spin-coating. The substrate was thermally annealed (180 ^oC for 5 min) in a glove-box. The ungrafted material was removed by repeated sonication in chloroform and then dried with nitrogen. The immobilization of NPs was performed by placing a droplet of the colloidal suspension on top of

the PEG-grafted substrates. All substrates were washed in water under sonication for 2 min following the immobilization process and dried with nitrogen.

2.4. Fabrication of nanoscale patterns of end-grafted PEG layers

The silicon substrates modified with end-grafted PEG layers were patterned using electrospun nanofibers as etch masks. Nanofibers of poly(ethylene oxide) (300 kg/mol) were electrospun from an aqueous solution (4.75%) on top of the PEG-grafted silicon substrates. Electrospinning was performed in the near-field regime at a substrate to nozzle distance of 1 mm and the substrate was moved at a lateral speed of 150 mm/s. The substrates were etched in oxygen plasma (45 s, ~100 mT, 5 sccm) to remove the end-grafted PEG layers that are not protected by the nanofibers. Further details of the patterning process can be found in our previous study [37].

2.5. Characterization of the substrates

The thickness of the end-grafted polymer layer was measured via ellipsometry (Gaertner, USA) at a fixed angle (70^o) of incidence. The substrate was modeled as silicon substrate / native silicon oxide layer (thickness of 1.5 nm, refractive index of 1.543) / PEG (refractive index of 1.46). The grafting density (Σ) was calculated using the equation given below. In the equation, h, ρ, N_A and M_n indicate the ellipsometric thickness, density of PEG (1.09 g/cm^3), Avagadro's number and number average molecular weight of the polymer, respectively.

$$\Sigma = h \cdot \rho \cdot N_A / M_n \qquad (1)$$

The surface topography of the end-grafted PEG layer was imaged in the dry state using AFM (Veeco Multimode 8, USA) in tapping mode. The morphology of the substrates following assembly of the particles was characterized with SEM (Zeiss EVO LS10, Germany) at 25 kV. The SEM images are representative of images taken from at least three different regions of the

substrate. SERS measurements were performed with a Witec alpha300 M+ model Raman spectrophotometer (Germany) equipped with a laser at a wavelength of 532 nm. Rhodamine 6G (Sigma-Aldrich) was dissolved in ethanol with concentrations that ranged from 10^{-5} M to 10^{-10} M. A drop with a volume of 3 μL was then deposited on the substrate. Raman scattering measurements were performed after drying of the solvent using 50× and 100× objectives with a spot size of 1 μm and an integration time of 0.05 s. The average spectra and intensities were obtained from Raman mappings over an area of 6 x 15 μm^2 with a step size of 0.5 μm.

3. Results and Discussion

3.1. Preparation of PEG grafted silicon substrates for assembly of gold NRs

Figure 1 presents important steps for the immobilization and assembly of gold NRs on substrates functionalized with end-grafted PEG layers. A film of PEG was first spin-coated on a freshly cleaned silicon substrate. A 5 min annealing at a temperature of 180 ^oC was sufficient for end-grafting of PEG via the condensation reaction between the surface silanol groups of the substrate and end-hydroxyl groups of the polymer [38]. The advantages of this grafting scheme for PEG include: i) availability of PEG with well-defined molecular weights with a low polydispersity index and high purity; ii) Since PEG is inherently terminated with hydroxyl groups, there is no need for post-functionalization of the polymer; and iii) The ability to generate uniform films over large areas. The removal of the unreacted polymers by sonication in chloroform leads to an end-grafted layer of PEG with an ellipsometric thickness of 12.0 ± 0.8 nm. The areal chain density calculated using Equation 1 was 0.22 chains/nm^2. The grafting density compares well with the end-grafted polymers that were reported to be in the brush regime [39]. The silicon substrates modified with the end-grafted layers of PEG displayed a highly smooth surface with a roughness lower than 1 nm (see supplementary Figure S1). Linear features in the AFM images arise as a

result of the crystallinity of the polymer [40]. PEG grafted substrates present binding sites for the immobilization of citrate-stabilized gold NRs, which are prepared by colloidal synthesis of CTAB-stabilized rods followed by a two-step ligand exchange process. A sonication assisted washing step following the deposition of citrate-stabilized gold NRs ensures removal of weakly bound particles from the PEG-grafted substrates.

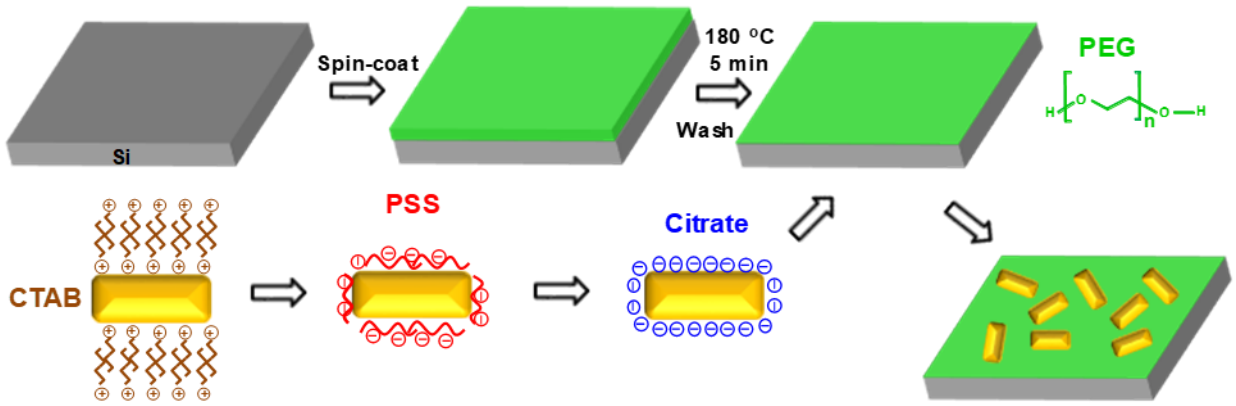

Figure 1. Schematic description of the process used for the assembly of gold NRs on PEG-grafted substrates.

3.2. Synthesis, Characterization and Immobilization of CTAB and Citrate-Stabilized Gold NRs

Gold NRs stabilized with two different ligands were prepared by wet-chemical synthesis. CTAB-stabilized gold NRs were prepared first through a seed-mediated growth approach. TEM images in Figure 2a show that the rods are ~50 nm in length and ~20 nm in width. UV-vis extinction spectra revealed characteristic peaks that correspond to ~625 nm and ~530 nm associated with the longitudinal and transverse plasmon resonances, respectively. The concentration of the rods was 95 mg/L as determined using inductively coupled plasma-mass-spectrometry. A recently [35] reported procedure was used for ligand exchange from CTAB to citrate. Here, CTAB was first removed through treatment with PSS which is later exchanged with citrate. The intermediate PSS

treatment is necessary for the completion of the ligand exchange process without aggregation of the particles. UV-vis extinction spectra of NRs revealed that there was a small red-shift due to the ligand exchange. The zeta potential measurements (see supplementary Table S1) further verified the ligand exchange process. Initially the CTAB-stabilized gold NRs were positively charged with a zeta potential of +50.1 ± 0.5 mV. Following the ligand exchange from CTAB to PSS, the gold NRs became negatively charged (- 51.7 ± 2.7 mV). The further replacement of PSS with citrate resulted in gold NRs with a slightly less negative surface charge (- 51.0 ± 3.7 mV).

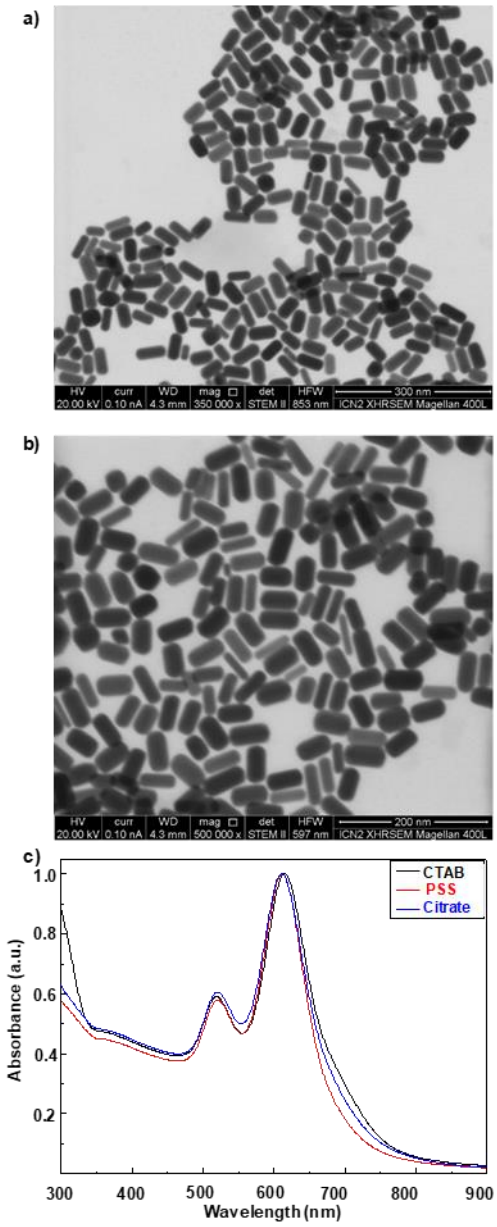

Figure 2. Gold NRs. a, b) TEM images of the rods at a) 350,000× and b) 500,000× magnification. c) UV-vis spectra of gold NRs with different ligands. The concentration of gold NRs was 95 mg/L.

The ligand plays a critical role in the interaction of gold NRs with end-grafted PEG layers. The same size of gold NRs stabilized with CTAB and citrate were immobilized on PEG-grafted silicon substrates for 24 h. The substrates were imaged with SEM following sonication in water and drying. CTAB-stabilized gold NRs did not bind to the PEG-grafted substrates, whereas the

citrate-stabilized ones immobilized uniformly over the substrates with an average particle density of 23 NRs/μm^2 (Figure 3). In the absence of end-grafted PEG layers, citrate stabilized gold NRs did not bind to the bare silicon substrates (Figure 3c). Results were similar for a batch of gold NRs (see supplementary Figure S2 for the TEM images and UV-Vis spectra) with a higher concentration (148 mg/L) of the particles. These results show that the ligand plays a critical role in the interaction of the particles with end-grafted PEG layers. It is likely that PEG chains cannot remove the CTAB ligands to interact with the bare gold surface, since the association of CTAB to the gold NRs is stronger than citrate. These results are in agreement with a previous study by Vaia and coworkers [23] who reported that mercaptopropanesulfonate capped spherical gold NPs did not immobilize on end-grafted PEG layers.

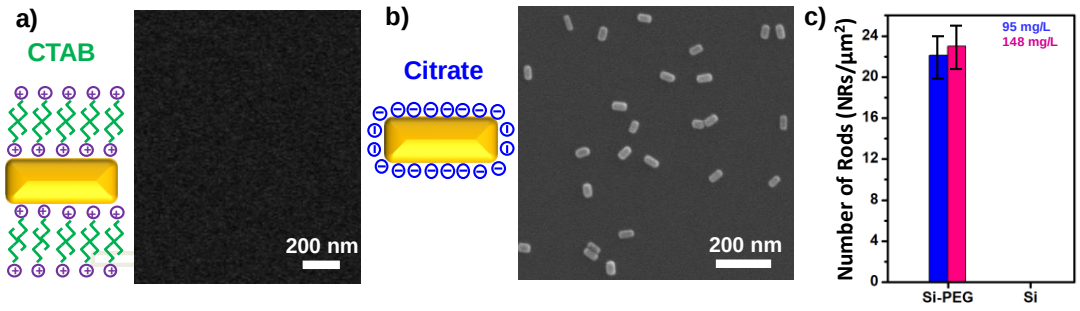

Figure 3. Immobilization of gold NRs on PEG-grafted substrates. SEM images of the substrates following immobilization of a) CTAB-stabilized and b) citrate-stabilized gold NRs. The SEM image given in part (a) shows that CTAB-stabilized gold NRs did not bind to PEG-grafted substrates. c) The density of citrate stabilized gold NRs immobilized on PEG-grafted and bare silicon substrates. The immobilization was performed for 24 h using two different concentrations of the rods..

3.3. Assembly of gold NRs on nanoscale patterns of PEG

Control over the position and orientation of gold NRs is critically important to tune their collective plasmonic properties for use in device applications. The selective immobilization of citrate-stabilized gold NRs on substrates modified with PEG together with demonstrated capabilities in fabricating nanoscale patterns of polymer thin films, open up a range of opportunities for the spatially defined assembly of plasmonic nanostructures. Herein, a versatile nanofabrication technique is utilized to prepare one-dimensional nanoscale patterns of end-grafted PEG layers. The method, sometimes referred to as electrospin nanolithography or organic nanowire lithography, relies on electrospun nanofibers as masks for selective material removal during oxygen plasma etching (Figure 4a) [37, 41]. Near-field electrospinning enables spatially defined and highly aligned deposition of nanofibers allowing fabrication of linear patterns of end-grafted PEG layers in regions that are protected by the nanofibers. The removal of nanofibers through repeated washing results in stripes of PEG with widths that are defined by the diameter of the fiber and etching conditions. Spotting a droplet of the suspension containing the citrate-stabilized gold NRs followed by washing in water under sonication results in linear arrays of the particles (Figure 4b). This result further highlights the specific interaction of citrate-stabilized gold NRs with end-grafted PEG layers, since rods selectively bound to the patterned regions with extremely low levels of non-specific adsorption to the background regions. We prepared a series of stripes with line widths ranging from ~400 nm to ~50 nm by varying the diameter of the nanofiber used to mask the underlying PEG layer (Figure 4c). The width of the pattern not only determined the number of rods immobilized per line width, but also affected the orientation of the rods. At wide lines, the orientation of the rods was mostly random and a significant fraction of the rods assembled with their long axis perpendicular to the direction of the pattern. This kind of packing was also observed

for the assembly of mercaptopropane sulfonate functionalized NRs on patterns of poly(2-vinylpyridine) surrounded by polystyrene regions [42]. Such assemblies likely result from the minimization of the interface between the rods and native oxide that is found in the background regions. The rods exhibited end-to-end type assemblies with single particle per width, when the width of the lines approached the length of the rods.

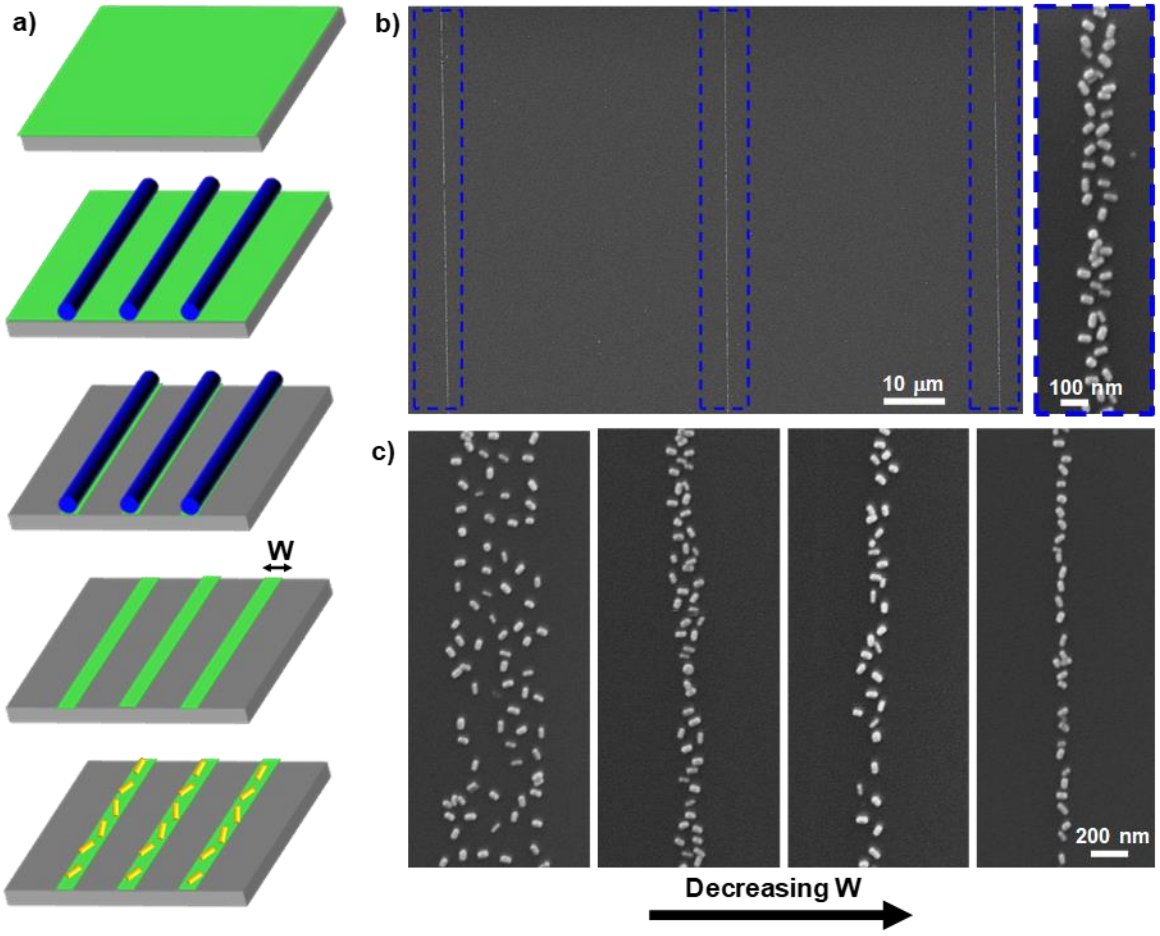

Figure 4. Assembly of citrate-stabilized gold NRs on linear nanoscale patterns of end-grafted PEG layers. a) Schematic description of electrospin nanolithography to fabricate nanopatterns. The process starts with a homogenous layer of end-grafted PEG followed by aligned deposition of electrospun nanofibers. Oxygen plasma etching removes end-grafted PEG layers that are not

protected by the nanofibers. Washing off the nanofibers results in arrays of stripes which constitute binding sites for selective immobilization of citrate-stabilized gold NRs. b,c) SEM images of b) arrays of patterned gold NRs, c) individual stripes of varying width.

A particular application of the presented platform is detection of molecules in Raman spectroscopy based on the enhancement of the signals near the gold NR assemblies. We probed the SERS activity of gold NRs assembled on PEG-grafted substrates by using rhodamine 6G as the reporter molecule under 532 nm laser excitation. Figure 5a presents the SERS spectrum of rhodamine 6G clearly exhibiting the fingerprint peaks at positions that are in good agreement with the literature [43]. Raman intensity mapping and SEM images (Figure 5b) show that the SERS response specifically emerges from the patterned gold NRs. This observation further verifies the selective immobilization of the citrate-stabilized gold NRs onto nanoscale patterns of PEG. To determine the detection limit of the fabricated SERS platform, we deposited different concentrations of rhodamine 6G on the both patterned and unpatterned PEG layers. Figure 5c shows the SERS spectra of rhodamine 6G on patterned gold NRs for deposition at concentrations ranging from 10 μM to 100 pM. The lowest concentration of the reporter molecule that could be clearly detected was 1 nM on the patterned NRs. This detection limit exceeds those obtained with surface-assemblies of gold nanostars [44], nanospheres [36], NRs [45], and core-shell nanoparticles [46]. Figure 5d compares the SERS intensity at 1365 cm^{-1} of the reporter molecule deposited on gold NRs immobilized on patterned and unpatterned PEG layers. The SERS activity of the NRs was consistently higher on the patterned substrates in comparison with the unpatterned ones for the entire range of the concentrations investigated. At a reporter concentration of 10 μM, for example, the intensity at 1365 cm^{-1} was 120 on the patterns whereas it was 10 on unpatterned substrates. On the unpatterned PEG grafted substrates, the fingerprint peaks were not clearly

distinguishable at concentrations lower than 1 μM. These results indicate that the assembly of gold NRs on the nanoscale patterns of PEG significantly increases SERS intensities and allow for detection of molecules at much lower concentrations in comparison with PEG grafted homogeneous substrates. This improvement can be explained by two effects. First, the density of the immobilized rods is significantly higher on the patterns in comparison with the homogenous PEG layers. The density of the gold NRs immobilized for 3h was typically ~30 NRs/ μm^2 on the patterned stripes in comparison with ~10 NRs/μm^2 on the unpatterned substrates prepared at identical conditions. This type of funneling effect was previously observed on nanopatterned PEG brushes with citrate-stabilized spherical gold NPs [37, 47]. The density of the particles contributes to SERS activity by increasing the number of scattering centers as well as by reducing the inter-particle distances favoring formation of plasmonic hot spots. The second effect contributing to SERS may relate to the assembly of nanorods at particular orientations resulting in strong focusing of electromagnetic fields near the ends of the rods.

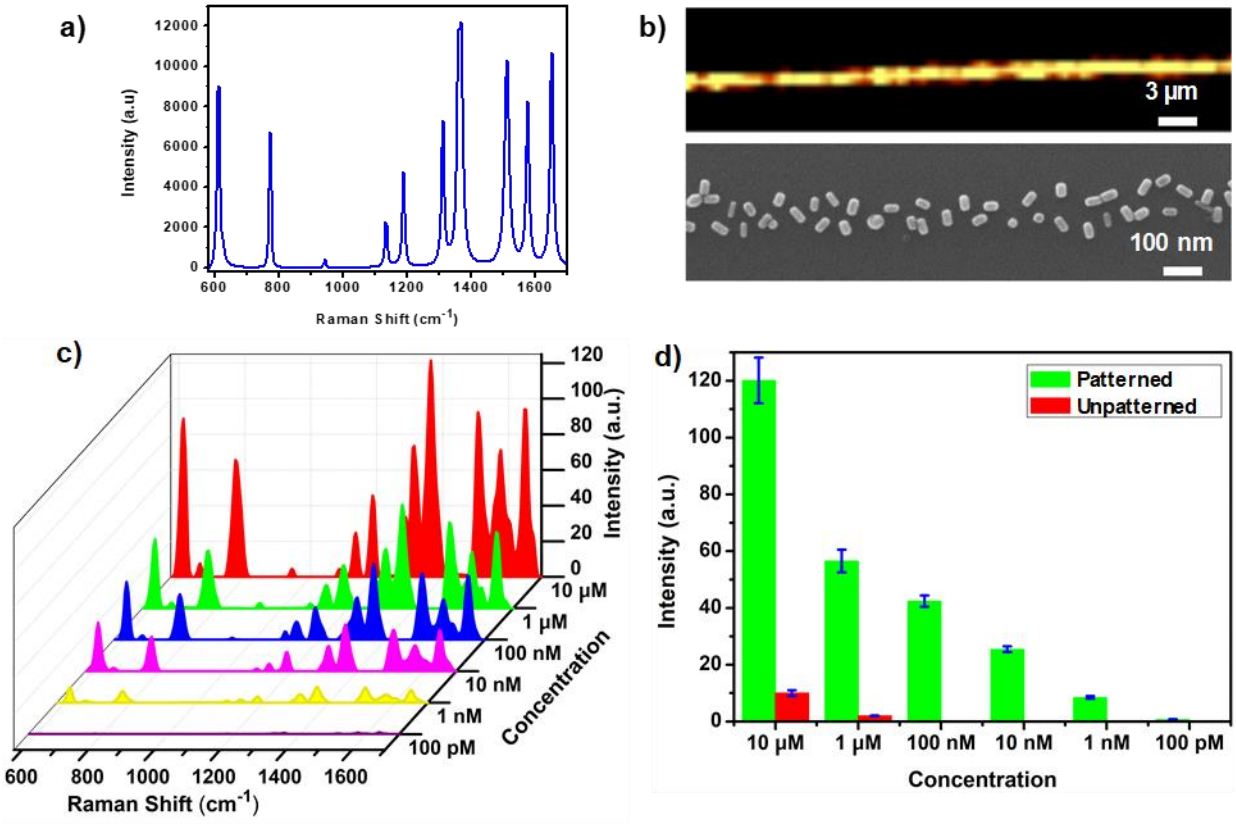

Figure 5. SERS properties of gold NRs assembled on nanopatterned PEG layers. a) SERS spectrum of rhodamine 6G at a concentration of 10 µM on gold NRs assembled on the patterned substrates. b) Raman mapping and SEM images of the patterned gold NRs. c) SERS spectra of rhodamine 6G for concentrations ranging between 10 µM and 100 pM. d) SERS intensities of rhodamine 6G as a function of its concentration on gold NRs immobilized on patterned and unpatterned PEG-grafted substrates. The mapping image and SERS intensities were obtained using the characteristic peak of rhodamine 6G at a position of 1365 cm^{-1}.

4. Conclusions

The results reported here demonstrate that colloidal chemistry and surface engineering approaches can be used together for tunable assembly of gold NRs on PEG-grafted solid substrates. The key in the first-time immobilization and assembly of colloidal gold NRs on end-grafted PEG layers

was tailoring the particle-substrate interactions via the exchange of ligands from CTAB to citrate. The selective particle-substrate interaction allowed for the spatially defined assembly of gold NRs on the linear nanoscale patterns of end-grafted PEG layers. The fundamental and technological importance of this study is the significant enhancement of the SERS activity of the gold NRs assembled on nanopatterned substrates. The close-placement of gold NRs at high densities over the patterned regions was critical in generating hot-spots as evidenced by SERS mapping images. The approaches reported in this study provide insights for modulating the collective properties of nanoparticles of varying shape and composition through directed self-assembly concepts.

AUTHOR INFORMATION

Corresponding Authors:

E-mail: onses@erciyes.edu.tr

E-mail: victor.puntes@icn2.cat

ACKNOWLEDGEMENTS

This work was supported by Research Fund of the Erciyes University (Project Number: FYL-2016-6896). ICN2 is supported by the Severo Ochoa program from Spanish MINECO (Grant No. SEV-2013-0295) and funded by the CERCA Programme / Generalitat de Catalunya.

Graphical Abstract

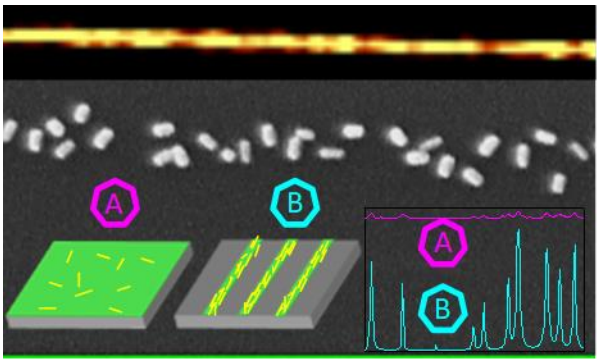

REFERENCES

[1] L.K. Bogart, G. Pourroy, C.J. Murphy, V. Puntes, T. Pellegrino, D. Rosenblum, D. Peer, R. Levy, Nanoparticles for Imaging, Sensing, and Therapeutic Intervention, Acs Nano, 8 (2014) 3107-3122.
[2] Y.H. Zheng, C. Jiang, S.H. Ng, Y. Lu, F. Han, U. Bach, J.J. Gooding, Unclonable Plasmonic Security Labels Achieved by Shadow-Mask-Lithography-Assisted Self-Assembly, Adv Mater, 28 (2016) 2330-2336.
[3] Y.H. Jang, Y.J. Jang, S. Kim, L.N. Quan, K. Chung, D.H. Kim, Plasmonic Solar Cells: From Rational Design to Mechanism Overview, Chem Rev, 116 (2016) 14982-15034.
[4] C. Zhang, H.Q. Zhao, L.A. Zhou, A.E. Schlather, L.L. Dong, M.J. McClain, D.F. Swearer, P. Nordlander, N.J. Halas, Al-Pd Nanodisk Heterodimers as Antenna-Reactor Photocatalysts, Nano Lett, 16 (2016) 6677-6682.
[5] P.K. Jain, K.S. Lee, I.H. El-Sayed, M.A. El-Sayed, Calculated absorption and scattering properties of gold nanoparticles of different size, shape, and composition: Applications in biological imaging and biomedicine, J Phys Chem B, 110 (2006) 7238-7248.
[6] N.D. Burrows, A.M. Vartanian, N.S. Abadeer, E.M. Grzincic, L.M. Jacob, W. Lin, J. Li, J.M. Dennison, J.G. Hinman, C.J. Murphy, Anisotropic nanoparticles and anisotropic surface chemistry, The journal of physical chemistry letters, 7 (2016) 632-641.
[7] J.M. Romo-Herrera, R.A. Alvarez-Puebla, L.M. Liz-Marzan, Controlled assembly of plasmonic colloidal nanoparticle clusters, Nanoscale, 3 (2011) 1304-1315.
[8] V.F. Puntes, P. Gorostiza, D.M. Aruguete, N.G. Bastus, A.P. Alivisatos, Collective behaviour in two-dimensional cobalt nanoparticle assemblies observed by magnetic force microscopy, Nat Mater, 3 (2004) 263.
[9] K.-Q. Lin, J. Yi, S. Hu, B.-J. Liu, J.-Y. Liu, X. Wang, B. Ren, Size Effect on SERS of gold nanorods demonstrated via single nanoparticle spectroscopy, The Journal of Physical Chemistry C, 120 (2016) 20806-20813.
[10] A.M. Funston, C. Novo, T.J. Davis, P. Mulvaney, Plasmon coupling of gold nanorods at short distances and in different geometries, Nano Lett, 9 (2009) 1651-1658.
[11] G. Demirel, H. Usta, M. Yilmaz, M. Celik, H.A. Alidagi, F. Buyukserin, Surface-enhanced Raman spectroscopy (SERS): an adventure from plasmonic metals to organic semiconductors as SERS platforms, J Mater Chem C, 6 (2018) 5314-5335.

[12] M. Kahraman, E.R. Mullen, A. Korkmaz, S. Wachsmann-Hogiu, Fundamentals and applications of SERS-based bioanalytical sensing, Nanophotonics-Berlin, 6 (2017) 831-852.
[13] J. Gopal, H.N. Abdelhamid, J.-H. Huang, H.-F. Wu, Nondestructive detection of the freshness of fruits and vegetables using gold and silver nanoparticle mediated graphene enhanced Raman spectroscopy, Sensors and Actuators B: Chemical, 224 (2016) 413-424.
[14] Ö. Aydin, M. Kahraman, E. Kiliç, M. Çulha, Surface-enhanced Raman scattering of rat tissues, Applied spectroscopy, 63 (2009) 662-668.
[15] M. Manikandan, H.N. Abdelhamid, A. Talib, H.-F. Wu, Facile synthesis of gold nanohexagons on graphene templates in Raman spectroscopy for biosensing cancer and cancer stem cells, Biosensors and Bioelectronics, 55 (2014) 180-186.
[16] K.D. Alexander, K. Skinner, S. Zhang, H. Wei, R. Lopez, Tunable SERS in gold nanorod dimers through strain control on an elastomeric substrate, Nano Lett, 10 (2010) 4488-4493.
[17] Y.Q. Chen, K.X. Bi, Q.J. Wang, M.J. Zheng, Q. Liu, Y.X. Han, J.B. Yang, S.L. Chang, G.H. Zhang, H.G. Duan, Rapid Focused Ion Beam Milling Based Fabrication of Plasmonic Nanoparticles and Assemblies via "Sketch and Peel" Strategy, Acs Nano, 10 (2016) 11228-11236.
[18] A. Genc, J. Patarroyo, J. Sancho-Parramon, N.G. Bastus, V. Puntes, J. Arbiol, Hollow metal nanostructures for enhanced plasmonics: synthesis, local plasmonic properties and applications, Nanophotonics-Berlin, 6 (2017) 193-213.
[19] M.S. Onses, L. Wan, X.Y. Liu, N.B. Kiremitler, H. Yilmaz, P.F. Nealey, Self-Assembled Nanoparticle Arrays on Chemical Nanopatterns Prepared Using Block Copolymer Lithography, Acs Macro Lett, 4 (2015) 1356-1361.
[20] V.F. Puntes, K.M. Krishnan, A.P. Alivisatos, Colloidal nanocrystal shape and size control: the case of cobalt, Science, 291 (2001) 2115-2117.
[21] J. Patarroyo, A. Genç, J. Arbiol, N.G. Bastús, V. Puntes, One-pot polyol synthesis of highly monodisperse short green silver nanorods, Chemical Communications, 52 (2016) 10960-10963.
[22] B. Yanez-Soto, S.J. Liliensiek, C.J. Murphy, P.F. Nealey, Biochemically and topographically engineered poly(ethylene glycol) diacrylate hydrogels with biomimetic characteristics as substrates for human corneal epithelial cells, J Biomed Mater Res A, 101 (2013) 1184-1194.
[23] S. Diamanti, S. Arifuzzaman, J. Genzer, R.A. Vaia, Tuning Gold Nanoparticle-Poly(2-hydroxyethyl methacrylate) Brush Interactions: From Reversible Swelling to Capture and Release, Acs Nano, 3 (2009) 807-818.
[24] X.Y. Liu, S. Biswas, J.W. Jarrett, E. Poutrina, A. Urbas, K.L. Knappenberger, R.A. Vaia, P.F. Nealey, Deterministic Construction of Plasmonic Heterostructures in Well-Organized Arrays for Nanophotonic Materials, Adv Mater, 27 (2015) 7314-+.
[25] S. Biswas, X.Y. Liu, J.W. Jarrett, D. Brown, V. Pustovit, A. Urbas, K.L. Knappenberger, P.F. Nealey, R.A. Vaia, Nonlinear Chiro-Optical Amplification by Plasmonic Nanolens Arrays Formed via Directed Assembly of Gold Nanoparticles, Nano Lett, 15 (2015) 1836-1842.
[26] M. Ben Haddada, M. Hübner, S. Casale, D. Knopp, R. Niessner, M. Salmain, S. Boujday, Gold Nanoparticles Assembly on Silicon and Gold Surfaces: Mechanism, Stability and Efficiency in Diclofenac Biosensing, The Journal of Physical Chemistry C, (2016).
[27] M.S. Onses, Fabrication of Nanopatterned Poly(ethylene glycol) Brushes by Molecular Transfer Printing from Poly(styrene-block-methyl methacrylate) Films to Generate Arrays of Au Nanoparticles, Langmuir, 31 (2015) 1225-1230.
[28] N. Meyerbroker, T. Kriesche, M. Zharnikov, Novel Ultrathin Poly(ethylene glycol) Films as Flexible Platform for Biological Applications and Plasmonics, Acs Appl Mater Inter, 5 (2013) 2641-2649.
[29] N. Meyerbroker, M. Zharnikov, Hydrogel Nanomembranes as Templates for Patterned Deposition of Nanoparticles on Arbitrary Substrates, Acs Appl Mater Inter, 6 (2014) 14729-14735.

[30] N. Meyerbroker, M. Zharnikov, Modification and Patterning of Nanometer-Thin Poly(ethylene glycol) Films by Electron Irradiation, Acs Appl Mater Inter, 5 (2013) 5129-5138.
[31] A.R. Ferhan, L.H. Guo, X.D. Zhou, P. Chen, S. Hong, D.H. Kim, Solid-Phase Colorimetric Sensor Based on Gold Nanoparticle-Loaded Polymer Brushes: Lead Detection as a Case Study, Anal Chem, 85 (2013) 4094-4099.
[32] M.-J. Lee, S.-H. Lim, J.-M. Ha, S.-M. Choi, Green Synthesis of High-Purity Mesoporous Gold Sponges Using Self-Assembly of Gold Nanoparticles Induced by Thiolated Poly (ethylene glycol), Langmuir, 32 (2016) 5937-5945.
[33] M. Sakir, S. Pekdemir, A. Karatay, B.l. Küçüköz, H.H. Ipekci, A. Elmali, G. Demirel, M.S. Onses, Fabrication of Plasmonically Active Substrates Using Engineered Silver Nanostructures for SERS Applications, Acs Appl Mater Inter, 9 (2017) 39795-39803.
[34] B. Nikoobakht, M.A. El-Sayed, Preparation and growth mechanism of gold nanorods (NRs) using seed-mediated growth method, Chem. Mater, 15 (2003) 1957-1962.
[35] J.G. Mehtala, D.Y. Zemlyanov, J.P. Max, N. Kadasala, S. Zhao, A. Wei, Citrate-stabilized gold nanorods, Langmuir, 30 (2014) 13727-13730.
[36] S. Pekdemir, S. Karabel, N.B. Kiremitler, X. Liu, P. Nealey, M.S. Onses, Modulating the kinetics of nanoparticle adsorption for simple and high yield fabrication of plasmonic heterostructures as SERS substrates, ChemPhysChem, (2017).
[37] N.B. Kiremitler, S. Pekdemir, J. Patarroyo, S. Karabel, I. Torun, V.F. Puntes, M.S. Onses, Assembly of Plasmonic Nanoparticles on Nanopatterns of Polymer Brushes Fabricated by Electrospin Nanolithography, Acs Macro Lett, 6 (2017) 603-608.
[38] N.A. Alcantar, E.S. Aydil, J.N. Israelachvili, Polyethylene glycol-coated biocompatible surfaces, J Biomed Mater Res, 51 (2000) 343-351.
[39] M. Kim, S.K. Schmitt, J.W. Choi, J.D. Krutty, P. Gopalan, From Self-Assembled Monolayers to Coatings: Advances in the Synthesis and Nanobio Applications of Polymer Brushes, Polymers-Basel, 7 (2015) 1346-1378.
[40] B. Zdyrko, S.K. Varshney, I. Luzinov, Effect of molecular weight on synthesis and surface morphology of high-density poly (ethylene glycol) grafted layers, Langmuir, 20 (2004) 6727-6735.
[41] Y. Lee, S.Y. Min, T.W. Lee, Large‐Scale Highly Aligned Nanowire Printing, Macromol Mater Eng, (2017).
[42] D. Nepal, M.S. Onses, K. Park, M. Jespersen, C.J. Thode, P.F. Nealey, R.A. Vaia, Control over Position, Orientation, and Spacing of Arrays of Gold Nanorods Using Chemically Nanopatterned Surfaces and Tailored Particle-Particle-Surface Interactions, Acs Nano, 6 (2012) 5693-5701.
[43] S. Shim, C.M. Stuart, R.A. Mathies, Resonance Raman Cross‐Sections and Vibronic Analysis of Rhodamine 6G from Broadband Stimulated Raman Spectroscopy, ChemPhysChem, 9 (2008) 697-699.
[44] Q.Q. Su, X.Y. Ma, J. Dong, C.Y. Jiang, W.P. Qian, A Reproducible SERS Substrate Based on Electrostatically Assisted APTES-Functionalized Surface-Assembly of Gold Nanostars, Acs Appl Mater Inter, 3 (2011) 1873-1879.
[45] L. Wu, Z. Wang, S. Zong, Y. Cui, Rapid and reproducible analysis of thiocyanate in real human serum and saliva using a droplet SERS-microfluidic chip, Biosensors and Bioelectronics, 62 (2014) 13-18.
[46] S.K. Cha, J.H. Mun, T. Chang, S.Y. Kim, J.Y. Kim, H.M. Jin, J.Y. Lee, J. Shin, K.H. Kim, S.O. Kim, Au-Ag Core-Shell Nanoparticle Array by Block Copolymer Lithography for Synergistic Broadband Plasmonic Properties, Acs Nano, 9 (2015) 5536-5543.
[47] M.S. Onses, P.F. Nealey, Tunable Assembly of Gold Nanoparticles on Nanopatterned Poly(ethylene glycol) Brushes, Small, 9 (2013) 4168-4174.